Thermal Management Optimization of Vehicle Exhaust Systems to Reduce Fire Hazard Risk

Rakib Hasan [1]*, Nusrat Jahan [2], Tanvir Ahmed [3], Farzana Rahman [4]
[1-4] Department of Mechanical Engineering, Bangladesh University of Engineering and Technology (BUET), Dhaka-1000, Bangladesh

* Corresponding Author: **Rakib Hasan; E-mail: rakib.hasan@buet.ac.bd**

Article Info

P-ISSN: 3051-3383
E-ISSN: 3051-3391
Volume: 05
Issue: 01
Received: 22-08-2024
Accepted: 24-09-2024
Published: 19-11-2024
Page No: 87-96

Abstract
Vehicle exhaust systems operate in a thermally severe environment where high exhaust-gas temperatures, compact underbody packaging, radiative exposure, and limited local cooling can combine to create fire-prone conditions. The greatest risk is concentrated in the exhaust manifold, close-coupled catalyst, and front-pipe region, where hot external surfaces can overheat nearby polymers, wiring, underbody coatings, leaked fluids, and combustible roadside material. This study presents a design-oriented numerical framework for reducing fire hazard risk through coordinated thermal management of the exhaust system. The framework integrates a one-dimensional gas-to-wall energy model, external convection-radiation analysis, view-factor-based assessment of adjacent panel heating, and a normalized fire-hazard index for screening design alternatives. A representative mid-size passenger-vehicle architecture was evaluated under a high-load baseline condition and an optimized condition combining a low-emissivity heat shield, thin insulation, airflow redirection, and improved stand-off distance from vulnerable underbody regions. For the modeled case, the peak exposed surface temperature in the manifold region decreased from 437.3 C to 390.6 C, while the peak adjacent underbody temperature above the same region decreased from 132.9 C to 61.9 C. The front-pipe adjacent temperature fell from 85.9 C to 51.8 C, and the weighted fire-hazard index decreased by 40.2% relative to the baseline. The results indicate that the most effective strategy is not uniform cooling of the entire exhaust line, but targeted reduction of radiative exposure and locally improved heat rejection around thermally dominant zones. The proposed framework provides a practical basis for early-stage decisions on exhaust routing, shielding, clearance, and material selection.

Keywords: vehicle exhaust system, thermal management, fire hazard, heat shield, catalytic converter, underbody temperature, thermal optimization

1. Introduction

Thermal management in vehicle exhaust systems is no longer only a durability issue; it is also a safety-critical design problem. In modern passenger vehicles, the exhaust manifold, catalyst, front pipe, floor pan, wiring harnesses, clips, brake lines, polymer shields, and acoustic layers are packaged within a narrow space envelope. That dense architecture improves emissions performance and packaging efficiency, but it also intensifies local thermal interaction and raises the likelihood of thermally driven fire scenarios if abnormal exposure pathways are not controlled carefully (Marshall *et al*., 2019 [32]; Hossain *et al*., 2023 [5]). Earlier work established that exhaust heat transfer must be treated as a coupled problem involving internal convection, wall conduction, external convection, and radiation, rather than as a simple pipe-cooling exercise. Subsequent studies showed that underhood and underbody airflow architecture strongly influences the thermal field, because local recirculation, shielding geometry, and nearby surfaces can amplify hot spots even when bulk gas temperature is already decreasing downstream.

Fire hazard pathways associated with hot exhaust hardware are especially important in real-world operation. Experimental and fire-investigation studies show that hot exhaust and catalyst surfaces can ignite leaked fluids, gasoline on metallic components, lubricating oils on hot surfaces, and dry grass or leaves beneath recently operated vehicles when local temperature and contact conditions are unfavorable (Morse *et al*., 2017 [40]; Bai *et al*., 2024 [42]). From a design perspective, that means surface temperature alone is not the only relevant metric; the direction of heat flow toward vulnerable targets also matters. A recurring weakness in industrial practice is that exhaust heat is often managed reactively. A prototype is tested, a local hot spot is detected, and a shield or patch is added late in development. That approach can solve an immediate problem, but it rarely clarifies why one zone is thermally dominant, how much each intervention contributes, or whether the final package will remain robust across different operating scenarios. Broader engineering work on smart manufacturing, digital monitoring, hybrid manufacturing, and advanced thermal materials reinforces the value of integrated, model-informed design rather than late corrective action (Hossain *et al*., 2021 [25]; Hossain *et al*., 2022 [19]; Hossain *et al*., 2023 [31]; Hossain *et al*., 2024 [13]; Hossain *et al*., 2024 [41]).

The objective of this paper is therefore to reformulate exhaust-system thermal safety as a structured optimization problem. Rather than treating shielding, insulation, stand-off distance, and local airflow management as isolated fixes, the study models them as coupled variables governing exposed surface temperature, adjacent panel heating, and a system-level fire-hazard index. At a broader systems level, thermal design decisions increasingly intersect with sustainability, manufacturing strategy, and whole-system performance goals across transportation applications (Marshall *et al*., 2019 [32]; Yuan *et al*., 2020 [33]; Chinchwade *et al*., 2024 [39]). The contribution of the paper is threefold. First, it develops a compact and physically interpretable calculation route for exhaust thermal behavior during a severe thermal load case. Second, it links that calculation route to a hazard-oriented metric rather than surface temperature alone. Third, it demonstrates that a focused package of low-emissivity shielding, limited insulation, view-factor reduction, and airflow management can reduce fire-prone exposure more effectively than uniform cooling applied everywhere.

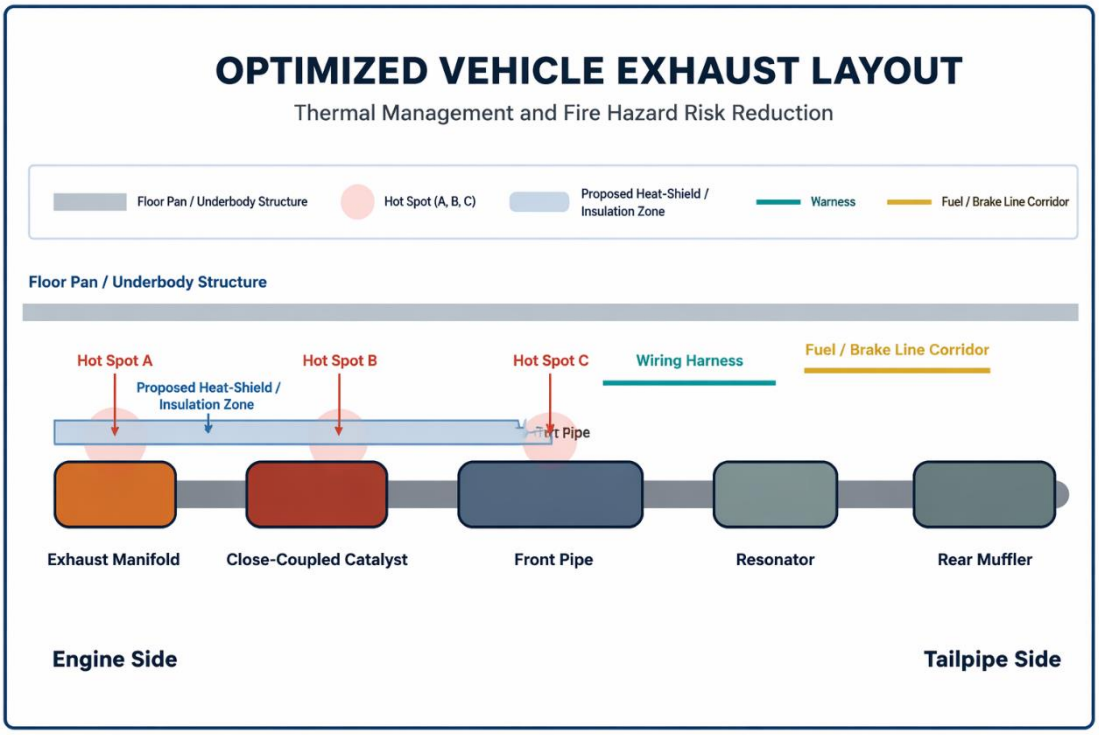

Fig 1: Representative exhaust architecture and the main thermally critical regions considered in the numerical study.

2. Literature review

Foundational studies by Konstantinidis *et al*. (1997 [1]) and Kandylas and Stamatelos (1999 [2]) demonstrated that automotive exhaust temperatures cannot be predicted adequately without accounting for transient internal convection, wall conduction, and radiation losses together further showed that exhaust-system thermal behavior is tightly coupled to catalyst heat-up and chemical conversion, especially during cold-start operation. Later reduced-order and hybrid studies extended this logic by showing that compact thermal models remain highly useful for early-stage vehicle thermal management when they preserve the dominant heat-transfer physics. Catalyst-focused modeling studies also confirmed that simplified dynamic and flow-sensitive representations can capture the connection between exhaust thermal behavior, converter response, and flow maldistribution.

The underhood literature expanded the problem from the exhaust line alone to the surrounding vehicle environment measured temperature and heat-flux distributions in a passenger-vehicle underhood compartment and showed that local airflow arrangements can unintentionally intensify downstream heating. Their later work on underhood control emphasized that airflow redirection and local deflection can materially improve thermal behavior while the subsequent review synthesized how component ordering, packaging density, and simplified modeling strategies shape whole-vehicle aerothermal performance. Comparable flow-network

and CFD-based approaches have likewise demonstrated the importance of coupling geometry with flow distribution in underhood thermal prediction. Shielding remains one of the most direct tools for limiting fire-prone thermal exposure. Lam *et al*. (2012 [8]) used CFD to show that properly located heat shields can reduce protected-zone temperatures and alter hot-air recirculation patterns developed exhaust-surface temperature models specifically for vehicle thermal-management simulations, highlighting the importance of configuration-specific treatment for exposed exhaust components. More recently, Dlugosz and Jarosz (2024 [11]) framed exhaust-shield design as an optimization problem, reinforcing the idea that shield geometry and surface properties should be selected systematically rather than by trial and error.

Recent studies also emphasize the value of combining reduced-order models with higher-fidelity simulation and optimization tools. Zhang *et al*. (2021 [9]) presented a systematic multi-objective optimization strategy for passenger-vehicle thermal management, while showed that CFD can clarify detailed temperature and flow behavior in exhaust hardware. Xiao (2015 [18]) demonstrated that fluid-solid coupling can improve transient exhaust thermal prediction, and Guardiola *et al*. (2016 [22]) showed how catalyst-inlet temperature estimation can support control-oriented thermal assessment. Together, these studies support a modeling hierarchy in which transparent engineering models guide early decisions and higher-fidelity tools refine the final package. Structural durability remains an essential companion problem that exhaust manifolds experience severe thermo-mechanical loading and that validation methodology must address fatigue-sensitive regions explicitly. Related material-focused studies on stainless steels and cast irons likewise underline that any thermal optimization must remain compatible with fatigue resistance, oxidation resistance, and long-term service durability. Despite this progress, an important gap remains between mainstream thermal studies and explicit fire-hazard interpretation. Many papers report temperatures, heat fluxes, catalyst performance, or durability metrics, but fewer translate those outputs into a design metric tied directly to hazardous exposure of adjacent components or combustible material. The present study addresses that gap by combining surface temperature prediction, adjacent panel heating, and a normalized fire-hazard index intended for screening design alternatives in early-stage vehicle development.

3. Methodology and governing equations

3.1. System definition and baseline configuration

Fig 1:

A representative front-engine passenger-vehicle exhaust layout was considered. The modeled exhaust line consists of an exhaust manifold, a close-coupled catalyst, a front pipe, a resonator, and a rear muffler. The analysis focuses on a high-load thermal condition because fire-hazard risk is most severe when gas temperature, wall temperature, radiative intensity, and proximity to vulnerable surfaces are elevated simultaneously. This type of system decomposition is consistent with earlier exhaust heat-transfer modeling approaches and later hybrid vehicle-thermal frameworks that prioritize dominant thermal resistances and geometry-dependent exposure paths (Chen, 1993 [15]; Konstantinidis *et al*., 1997 [1]; Ahmed *et al*., 2022 [20]).The numerical study is intentionally positioned as a design-screening model rather than a full durability or certification campaign. The aim is to retain the dominant physics needed for routing, shielding, and material-selection decisions while keeping the required inputs modest enough for early design use (Hossain *et al*., 2021 [25]; Hossain *et al*., 2022 [19])

3.2. NFPA 921: Guide for Fire and Explosion Investigations, 2024 Edition - Chapter 26 Motor Vehicle Fires

Table 26.3.1 Properties of Ignitible Liquids

	Flash Point [a]		Autoignition Temperature [b]		Flammability Limits [c]		Boiling Point [d]				Specific Gravity[e]
					LFL	UFL	IBP		FPB		
Liquid	°C	°F	°C	°F	%	%	°C	°F	°C	°F	(Air = 1)
Gasoline	−45 to −40	−49 to −40	350–460	660–860	1.4	7.6	26–49	78–120	171–233	339–452	3–4
Diesel fuel (fuel oil #2)	38–62	100–145	254–260	489–500	0.4	7	127–232	260–450	357–404	675–760	5–6
Brake fluid	110–171	230–340	300–319	572–606	1.2	8.5	232–288	111–142	460–550	238–288	5–6
Power steering fluid	175–180	347–356	360–>382	680–>720	1	7	309–348	588–658	507–523	945–973	>1
Motor oil	200–280	392–536	340–360	644–680	1	7	299–333	570–631	472–513	882–955	>1
Gear oil	150–270	302–510	>382	>716	1	7	316–371	601–700	>525	>977	>1
Automatic transmission fluid	150–280	302–536	330–>382	626–>716	1	7	239–242	462–468	507–523	945–973	>1
Ethylene glycol (antifreeze)	110–127	230–261	398–410	748–770	3.2	15.3	196–198	385–388			2.1
Propylene glycol (antifreeze)	93–107	199–225	371–421	700–790	2.6	12.5	187–188	369–370			2.6
Methanol (washer fluid)	11–15	52–55	464–484	867–903	6	36	65	149			1.1

Fig 1:

Table 1: Baseline operating and geometric parameters used in the numerical case study.

Parameter	Value	Unit	Description
Inlet exhaust gas temperature, T_g,in	900	°C	High-load representative condition
Exhaust mass flow rate, ṁ	0.030	kg s^{-1}	Representative gasoline-engine load point
Ambient temperature, T_∞	35	°C	Summer underbody environment
External underbody airflow speed	9.5	m s^{-1}	Baseline case
Manifold inner diameter	42	mm	Single-wall equivalent
Catalyst body diameter	95	mm	Close-coupled unit
Front-pipe inner diameter	50	mm	Unshielded baseline section

3.3. One-dimensional gas-to-wall energy model

The exhaust line is treated as a sequence of axially discretized control volumes. For each differential segment, the exhaust gas loses energy to the wall and then to the surroundings through external convection and radiation. This one-dimensional gas-to-wall treatment follows the engineering logic used in classic exhaust-system thermal studies, while remaining suitable for design-space screening before full CFD deployment (Konstantinidis *et al*., 1997 [1]; Kandylas & Stamatelos, 1999 [2]; Chen, 1993 [15]).

$$\dot{m}\, c_p \left(dT_g/dx\right) = - U P \left(T_g - T_\infty\right)$$

where m_dot is exhaust mass flow rate, c_p is gas specific heat, U is the overall heat-transfer coefficient, P is the effective wetted perimeter, and T_g and T_inf are the local gas and ambient temperatures, respectively. In practice, this overall form remains useful because it captures how internal convection, wall resistance, and ambient-side transfer interact in a way that is directly interpretable for design trade-offs (Depcik & Assanis, 2002 [34]; Wendland, 1993 [38]).

The internal convective coefficient is estimated using a Dittus-Boelter form for turbulent internal flow. This class of correlation remains widely used in compact exhaust modeling because it provides a reasonable balance between physical fidelity and computational simplicity for engineering studies of pipe-side heat rejection (Kandylas & Stamatelos, 1999 [2]; Depcik & Assanis, 2002 [34]).

$$Nu_i = 0.023\, Re_i^{0.8}\, Pr^{0.4}$$

$$h_i = (Nu_i\, k_g) / D_i$$

The overall resistance between the gas and the surroundings is expressed as the sum of gas-side, wall, optional insulation, and ambient-side resistances. In fire-oriented exhaust design, this resistance-network view is especially useful because it reveals whether a given intervention mainly alters gas cooling, outward leakage, or protected-side exposure (Konstantinidis *et al*., 1997 [1]; Abishek *et al*., 2020 [10]).

$$1/U = 1/h_i + (t_w/k_w) + R_{ins} + 1/(h_o + h_r)$$

The external forced-convection coefficient is calculated using a Churchill-Bernstein type cylinder correlation, while radiation is represented by an effective linearized radiative coefficient. Radiation is essential in the present application because radiative heat transfer often dominates the local exposure of nearby underbody parts when clearances are small and surface temperatures are high (Lam *et al*., 2012 [8]; Haehndel *et al*., 2013 [16]; Haehndel *et al*., 2014 [17]).

$$Nu_o = 0.3 + [0.62\ Re_o^{0.5}\ Pr^{(1/3)}] / [1 + (0.4/Pr)^{(2/3)}]^{(1/4)} \cdot [1 + (Re_o/282000)^{(5/8)}]^{(4/5)}$$

$$h_r = \varepsilon\ \sigma\ (T_s + T_\infty)(T_s^2 + T_\infty^2)$$

The exposed outer-surface temperature is obtained from the local partition of thermal resistances between the gas side and the ambient side. In the catalyst zone, an additional source term is included to represent exothermic oxidation of residual species, which helps explain why the close-coupled after-treatment region can remain thermally active even after bulk gas temperature begins to decline (Chan & Hoang, 1999 [3]; Peyton Jones *et al*., 2000 [23]; Shaw *et al*., 2002 [24]).

3.3. Adjacent panel heating and local fire-hazard metric

Because ignition risk depends on what the hot component is heating, a second calculation layer evaluates the temperature of nearby underbody panels and vulnerable components. This is consistent with fire-oriented evidence showing that hazardous outcomes are driven not only by the temperature of the exhaust hardware itself, but also by whether the thermal load is transferred efficiently toward combustible or temperature-sensitive targets (Morse *et al*., 2017 [40]; Bai *et al*., 2024 [42]; LaPointe *et al*., 2006 [43]).

$$q''_{adj} = F_{s\text{-}a}\ \varepsilon\ \sigma\ (T_s^4 - T_{adj}^4) + h_{gap}\ (T_{air,gap} - T_{adj})$$

where $F_{s\text{-}a}$ is an effective radiative view factor between the exhaust surface and the adjacent panel, and h_{gap} is a gap-scale coefficient representing local convective exchange in the narrow space between the hot part and the protected surface. In early design work, view-factor treatment is especially valuable because routing and shield position can change hazardous exposure even when the external metal temperature changes only modestly (Lam *et al*., 2012 [8]; Dlugosz & Jarosz, 2024 [11]).

A normalized fire-hazard index (FHI) is defined to compare design options on a common basis. The metric is intentionally simple: it blends adjacent-target temperature with exposed-surface temperature so that design screening does not focus exclusively on the exhaust metal while overlooking the protected side of the package. This type of composite metric is aligned with modern vehicle thermal optimization practice, where multiple competing objectives must be balanced rather than minimized one at a time (Hossain *et al*., 2023 [31]; Hossain *et al*., 2024 [13])

$$FHI = \Sigma_j\ w_j\ [0.6\ (T_{adj,j} / T_{lim,adj,j}) + 0.4\ (T_{s,j} / T_{lim,s,j})]$$

Here, j denotes each thermally relevant exhaust zone, w_j is a weighting factor, $T_{adj,j}$ is the predicted temperature of the adjacent surface, and T_{lim} terms are design-limit temperatures for the corresponding zone. Higher weighting is assigned to the manifold, catalyst, and front-pipe region because those zones are hotter, more radiatively intense, and typically closer to sensitive underbody content than the resonator or rear muffler

Table 2: Optimization variables used in the proposed thermal-management strategy.

Design variable	Symbol	Range / selected value	Purpose
Low-emissivity shield outer surface	ε	0.82 -> 0.38-0.48	Reduce radiative exchange
Local insulation / thermal resistance	R_ins	0 -> 0.020-0.030	Limit outward heat leakage
Underbody airflow redirection	h_o multiplier	1.00 -> 1.03-1.10	Increase convective removal
Effective stand-off / view-factor reduction	F_s-a	0.30-0.40 -> 0.14-0.20	Reduce local panel exposure

The optimization objective is to minimize FHI while maintaining practical packaging constraints and preserving after-treatment functionality. The optimized case therefore uses moderate shielding and airflow changes rather than unrealistically aggressive cooling. This reflects the real engineering target: the exhaust should remain thermally effective for emissions control, but it should direct less hazardous heat toward the surrounding structure (Hossain *et al*., 2024 [41]).

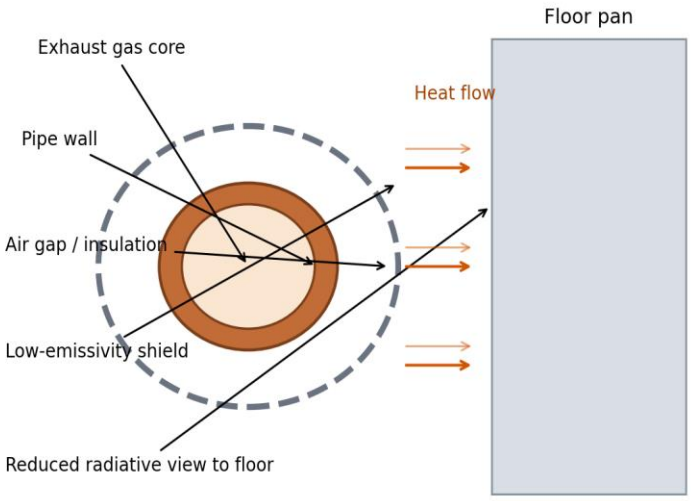

Fig 2: Cross-sectional thermal-management concept showing the pipe, stand-off, low-emissivity shield, and the protected floor-pan side.

3.5. Sample calculation

To illustrate the calculation route, consider the manifold section with D_i = 0.042 m, T_g approximately 850-900 C, m_dot = 0.030 kg s^-1, and ambient temperature of 35 C. Using the representative gas properties adopted in the model yields Re_i approximately 1.79 x 10^4 and Nu_i approximately 50.4, which corresponds to an internal convective coefficient of about h_i approximately 85 W m^-2 K^-1. For the baseline underbody airflow condition, the external correlation gives h_o approximately 57 W m^-2 K^-1, while the linearized radiative coefficient in the hot manifold region is on the order of h_r approximately 28 W m^-2 K^-1. These relative magnitudes are consistent with the literature, which repeatedly shows that radiation cannot be neglected in hot exhaust zones when surface temperatures are high and nearby targets are closed.

4. Results and discussion

The results are presented for two cases: a baseline architecture without dedicated low-emissivity shielding in the front hot zone, and an optimized architecture with targeted shielding, moderate insulation, and improved local airflow management. The comparison focuses on exposed outer-surface temperature, adjacent panel heating, and the resulting fire-hazard index. This framing is consistent with the literature showing that effective thermal management should be evaluated using both source-side and protected-side metrics.

4.1. Baseline thermal behavior

The baseline solution shows that the manifold and front-pipe region dominate the thermal field. The highest exposed outer-surface temperature occurs in the manifold, where the model predicts 437.3 C. The front pipe remains the second most severe region at 388.8 C, while the close-coupled catalyst stays thermally active but, in the modeled configuration, is partially moderated by its larger body area and surrounding geometry. That ordering is consistent with earlier studies indicating that the front hot zone is usually governed by a combination of high gas temperature, compact packaging, and strong local radiation. More important from a fire-risk perspective is the adjacent underbody response. The local panel above the manifold reaches 132.9 C in the baseline case, which is markedly more critical than the downstream resonator or muffler zones. The front-pipe adjacency also reaches 85.9 C, which is high enough to justify concern for nearby polymeric clips, wiring looms, local coatings, or combustible contamination. This confirms the central fire-

safety point of the paper: the most hazardous zone is not defined by exhaust metal temperature alone, but by the combination of local temperature and exposure pathway toward vulnerable.

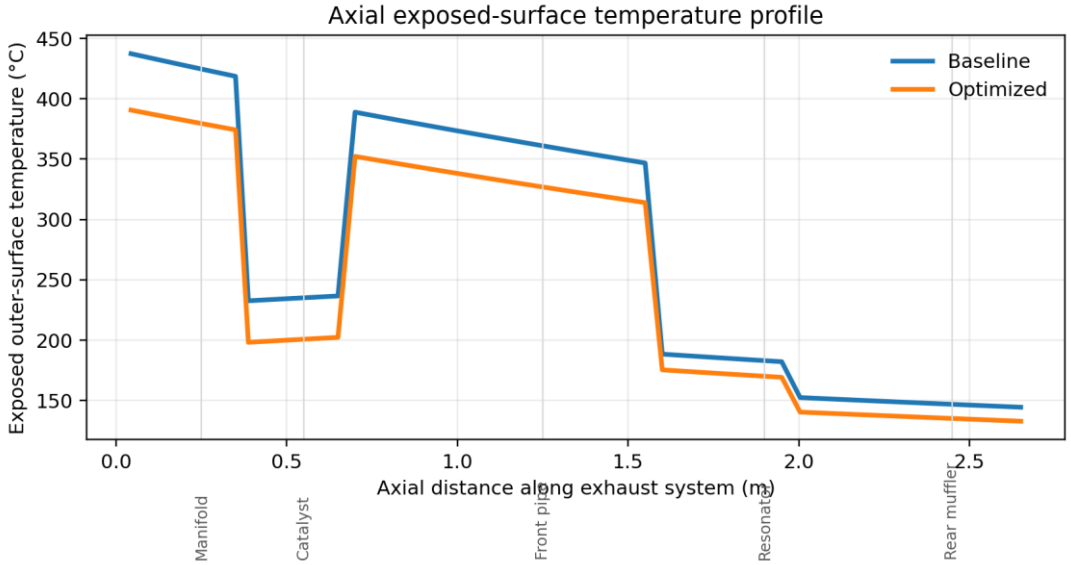

Fig 3: Baseline and optimized exposed-surface temperature profiles along the exhaust system.

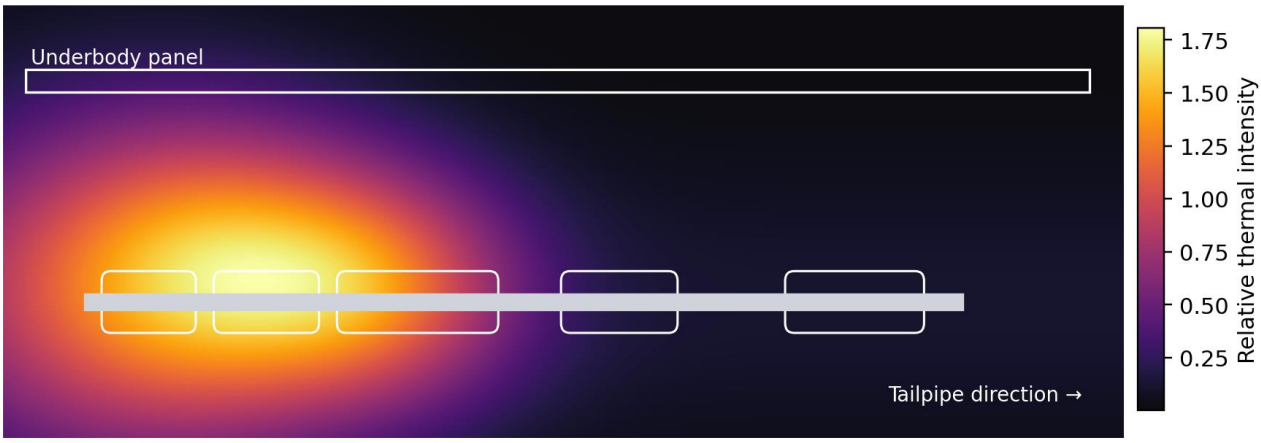

Fig 4: Conceptual baseline thermal map showing how the front hot zone dominates the underbody heat field.

4.2. Effect of shielding and local airflow management

The optimized design does not attempt to reduce every surface temperature by the same amount. Instead, it focuses on lowering radiative exposure in the dominant hot zones. In the manifold region the exposed temperature decreases from 437.3 C to 390.6 C, corresponding to a reduction of 10.7%. In the front pipe, the decrease is from 388.8 C to 352.2 C, or 9.4%. Those reductions are meaningful, but the larger safety benefit emerges in the protected region because shielding and view-factor control alter the direction of heat transfer more strongly than they alter the metal temperature itself (Lam *et al.*, 2012 [8]; Dlugosz & Jarosz, 2024 [11]; Haehndel *et al.*, 2014 [17]). The larger benefit appears on the protected side of the system. The adjacent panel temperature above the manifold falls from 132.9 °C to 61.9 °C, a reduction of 53.4%, while the front-pipe adjacent temperature falls from 85.9 °C to 51.8 °C, a reduction of 39.7%. This contrast between moderate surface cooling and much larger adjacent-target cooling is one of the most important design insights of the study. It shows that low emissivity, stand-off distance, and shield placement can deliver disproportionately strong safety gains by interrupting radiative transfer to nearby structures, which is especially important where hot surfaces may interact with combustible deposits or vulnerable materials (Lam *et al.*, 2012 [8]; Haehndel *et al.*, 2013 [16]; Morse *et al.*, 2017 [40]).

Physically, the result is sensible. A low-emissivity shield reduces radiative exchange, added thermal resistance limits direct outward leakage, and airflow redirection helps sweep heat away from the shielded zone. The measures act synergistically rather than independently, which is consistent with optimization studies showing that thermal-management improvements are often strongest when geometry, surface properties, and local flow are adjusted together rather than in isolation.

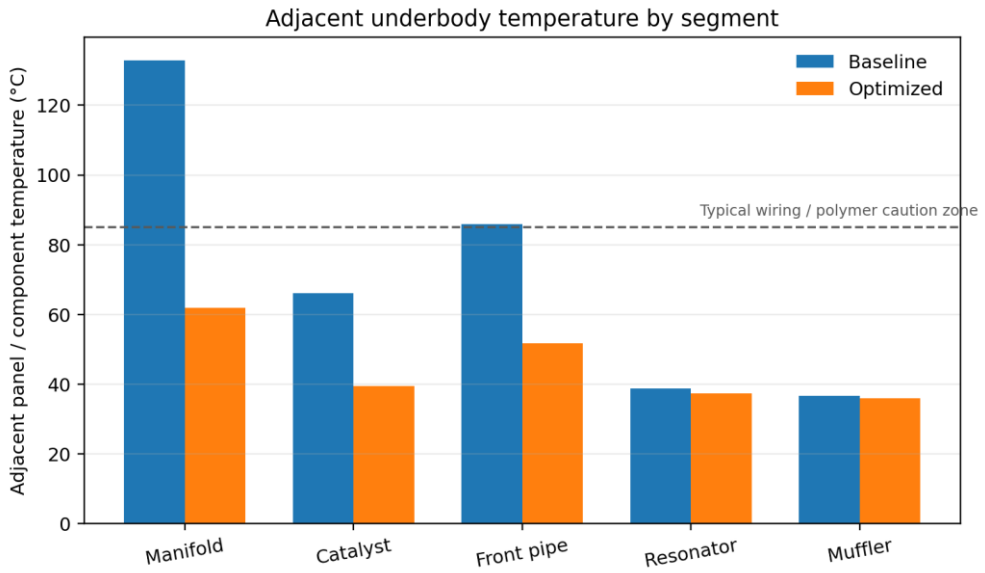

Fig 5: Comparison of adjacent underbody temperatures for the baseline and optimized cases.

4.3. Segment-wise hazard distribution and optimization outcome

The segment-wise hazard breakdown confirms that the manifold is the dominant contributor in the baseline architecture, followed by the front pipe and the catalyst. The muffler and resonator remain thermally relevant for durability, but their contribution to immediate fire-prone exposure is much smaller in the modeled vehicle. This ranking is consistent with both geometric proximity and the higher radiative intensity of the front hot zone, and it aligns with reported failure and durability concerns in manifolds and close-coupled exhaust hardware (Lorenzini *et al*., 2023 [12]; Santacreu *et al*., 2006 [27]; Mellouli *et al*., 2011 [28]).

When the weighted hazard metric defined in Eq. (8) is normalized by the baseline case, the optimized layout yields a hazard index of 0.60. In other words, the proposed package reduces the modeled thermal fire-hazard potential by 40.2% without requiring a wholesale redesign of the exhaust route. For early-stage vehicle development, that magnitude of reduction is meaningful because it suggests that targeted thermal design can avoid repeated downstream patchwork changes and simultaneously improve durability margins in the most critical front-end zones.

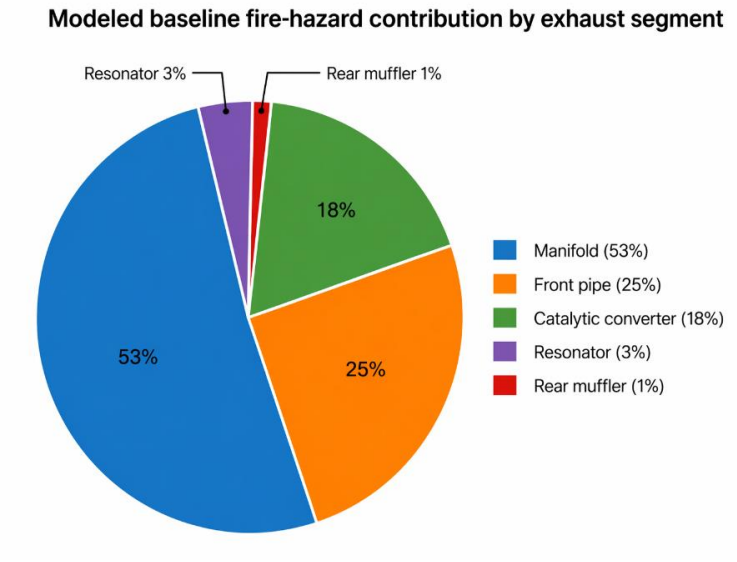

Fig 6: Modeled baseline hazard contribution by exhaust segment.

Table 3: Key thermal and hazard metrics for the baseline and optimized designs.

Metric	Baseline	Optimized	Change (%)
Manifold surface peak	437.3	390.6	-10.7
Front-pipe surface peak	388.8	352.2	-9.4
Manifold adjacent panel	132.9	61.9	-53.4
Front-pipe adjacent panel	85.9	51.8	-39.7
Normalized hazard index	1.00	0.60	-40.2

4.4. Engineering interpretation

Several engineering implications follow from the results. First, the most effective thermal fix is highly localized: the manifold-front-pipe zone deserves priority because it dominates both exposed temperature and underbody heating. Second, a moderate reduction in exposed metal temperature can translate into a much larger reduction in adjacent-component temperature when emissivity and view-factor management are optimized. Third, exhaust fire-risk mitigation should be evaluated at the system level. A cooler exhaust surface is helpful, but the true safety question is whether the surrounding structure, coatings, wiring, and nearby combustible matter remain below critical exposure limits under severe operating conditions (Marshall *et al*., 2019 [32]; Morse *et al*., 2017 [40]; Bai *et al*., 2024 [42]).

The numerical framework used here is deliberately compact, so it has clear limitations. The analysis does not include a full transient drive cycle, detailed after-treatment chemistry, leaked-fluid experiments, vegetation ignition experiments, or full-vehicle CFD of the underbody flow. Accordingly, the present study should be interpreted as a design-screening paper rather than a certification model. Even so, the structure of the results is robust enough to guide where shielding, clearance, airflow redirection, and material upgrades should be concentrated before more expensive validation stages are undertaken.

5. Conclusions

This paper presented a design-oriented numerical framework for reducing fire hazard risk in passenger-vehicle exhaust systems through coordinated thermal management. The study combined a one-dimensional exhaust heat-transfer model, local convection-radiation analysis, adjacent panel exposure prediction, and a normalized hazard index intended for early-stage design screening.

The modeled results show that the manifold and front-pipe region are the dominant fire-prone zones in the representative vehicle architecture. In the baseline case, the manifold surface reached 437.3 C and the adjacent underbody panel above that region reached 132.9 C. After optimization through low-emissivity shielding, modest insulation, airflow redirection, and reduced radiative view toward nearby panels, the manifold adjacent temperature decreased to 61.9 C and the normalized hazard index fell to 0.60 of the baseline value. The central finding is that fire-risk mitigation is governed less by uniform cooling of the full exhaust line and more by targeted control of radiative exposure in locally dominant hot zones. In practical vehicle design, this means that heat-shield surface properties, local stand-off distance, and airflow routing can be more influential than simply increasing metal thickness or applying late corrective patches.

Future work should extend the framework to transient drive cycles, misfire scenarios, leaked-fluid exposure, and coupled thermo-mechanical durability constraints. Even in its present form, however, the framework provides a clear and physically grounded route for integrating thermal safety into exhaust-system layout decisions in a way that is compatible with modern thermal-management, durability, and manufacturing workflows.

References

1. Konstantinidis PA, Koltsakis GC, Stamatelos AM. Transient heat transfer modelling in automotive exhaust systems. *Proc Inst Mech Eng Part C*. 1997;211(1):1–14. doi:10.1243/0954406971521610
2. Kandylas IP, Stamatelos AM. Engine exhaust system design based on heat transfer computation. *Energy Convers Manag*. 1999;40(10):1057–1072. doi:10.1016/S0196-8904(99)00008-4
3. Chan SH, Hoang DL. Heat transfer and chemical reactions in exhaust system of a cold-start engine. *Int J Heat Mass Transf*. 1999;42(22):4165–4183. doi:10.1016/S0017-9310(99)00064-2
4. Khaled M, Harambat F, Peerhossaini H. Underhood thermal management: temperature and heat flux measurements and physical analysis. *Appl Therm Eng*. 2010;30(6–7):590–598. doi:10.1016/j.applthermaleng.2009.11.003
5. Hossain MA, Dangol S, Hasan DW, Badugu D. Thermal performance study of additively manufactured compact heat exchangers for industrial energy systems. *J Mech Civ Ind Eng*. 2023;4(4):86–103. doi:10.32996/jmcie.2023.4.4.9
6. Khaled M, Harambat F, Peerhossaini H. Towards the control of car underhood thermal conditions. *Appl Therm Eng*. 2011;31(5):902–910. doi:10.1016/j.applthermaleng.2010.11.013
7. Khaled M, Ramadan M, El-Hage H, Elmarakbi A, Harambat F, Peerhossaini H. Review of underhood aerothermal management: towards vehicle simplified models. *Appl Therm Eng*. 2014;73(1):842–858. doi:10.1016/j.applthermaleng.2014.08.037
8. Lam SY, Shuaib NH, Hasini H, Shuaib NA. Computational fluid dynamics investigation on the use of heat shields for thermal management in a car underhood. *Int J Automot Mech Eng*. 2012;6:785–796. doi:10.15282/ijame.6.2012.10.0064
9. Zhang J, Wang Q, Shu CM, Zhang M, Lin J. A multi-objective optimization method for under-the-hood thermal management of vehicles. *Appl Therm Eng*. 2021;192:116818. doi:10.1016/j.applthermaleng.2021.116818
10. Abishek S, Balachandar R, Barron R. Quasi-1D model for exhaust gas and pipe with convective and temperature dependent emissivity based radiative heat losses. *Therm Sci Eng Prog*. 2020;18:100500. doi:10.1016/j.tsep.2020.100500
11. Dlugosz A, Jarosz J. Optimal design of selected features of exhaust system shields using different optimization methods and artificial neural networks. *Multiscale Multidiscip Model Exp Des*. 2024. doi:10.1007/s41939-024-00514-3
12. Lorenzini M, Barbieri SG, Mangeruga V, Giacopini M. Development of an experimental/numerical validation methodology for the design of exhaust manifolds of high performance internal combustion engines. *Eng Fail Anal*. 2023;154:107526. doi:10.1016/j.engfailanal.2023.107526
13. Hossain MA, Bhuiyan MAA, Rahman A, Hasan DW. Integration of artificial intelligence for real-time monitoring and process control in metal additive manufacturing systems. *J Mech Civ Ind Eng*. 2024;5(3):8–28. doi:10.32996/jmcie.2024.5.3.2
14. Shayler PJ, Hayden DJ, Ma T. Exhaust system heat transfer and catalytic converter performance. SAE Technical Paper 1999-01-0453; 1999. doi:10.4271/1999-01-0453
15. Chen DKS. A numerical model for thermal problems in

exhaust systems. SAE Technical Paper 931070; 1993. doi:10.4271/931070
16. Haehndel K, Frank T, Christel F, Spengler C, Suck G, Abanteriba S. Development of exhaust surface temperature models for 3D CFD vehicle thermal management simulations. Part 1: General exhaust configurations. *SAE Int J Passeng Cars Mech Syst*. 2013;6(2):847–858. doi:10.4271/2013-01-0879
17. Haehndel K, Jefferies A, Schlipf M, Frank T, Christel F, Abanteriba S. Development of exhaust surface temperature models for 3D CFD vehicle thermal management simulations. Part 2: Exhaust acoustic silencer configurations. SAE Technical Paper 2014-01-0646; 2014. doi:10.4271/2014-01-0646
18. Xiao G. Transient simulation of heat transfers for vehicle exhaust system. *Procedia Eng*. 2015;126:410–415. doi:10.1016/j.proeng.2015.11.233
19. Hossain MA, Barman SC, Pi W, Islam SMT. Hybrid manufacturing systems integrating additive manufacturing and CNC machining for high-precision industrial component production. *J Mech Civ Ind Eng*. 2022;3(2):24–41. doi:10.32996/jmcie.2022.3.2.4
20. Ahmed S, Rottengruber H, Full M. Hybrid model for exhaust systems in vehicle thermal management simulations. *Automot Engine Technol*. 2022;7:115–136. doi:10.1007/s41104-022-00104-w
21. Fernandez-Yanez P, Armas O, Gomez A, Gil A. Developing CFD models to evaluate available energy in exhaust systems of diesel light-duty vehicles. *Appl Sci*. 2017;7(6):590. doi:10.3390/app7060590
22. Guardiola C, Dolz V, Pla B, Mora J. Fast estimation of diesel oxidation catalysts inlet gas temperature. *Control Eng Pract*. 2016;56:148–156. doi:10.1016/j.conengprac.2016.08.020
23. Peyton Jones JC, Roberts J, Bernard P, Jackson RA. A simplified model for the dynamics of a three-way catalytic converter. SAE Technical Paper 2000-01-0652; 2000. doi:10.4271/2000-01-0652
24. Shaw BT, Fischer GD, Hedrick JK. A simplified cold-start catalyst thermal model to reduce hydrocarbon emissions. *IFAC Proc Vol*. 2002;35(1):307–312. doi:10.3182/20020721-6-ES-1901.01519
25. Hossain MA, Pi W, Islam SMT, Lide MI. Smart manufacturing framework for real-time process monitoring, predictive maintenance, and quality control. *J Mech Civ Ind Eng*. 2021;2(1):11–24. doi:10.32996/jmcie.2021.2.1.3
26. Santacreu PO, Cleizergues O, Simon C, Duroux P. Design of stainless steel automotive exhaust manifolds. *Rev Metall*. 2004;101(7):615–620. doi:10.1051/metal:2004130
27. Santacreu PO, Bucher L, Koster A, Remy L. Thermomechanical fatigue of stainless steels for automotive exhaust systems. *Rev Metall*. 2006;103(1):37–42. doi:10.1051/metal:2006102
28. Mellouli D, Haddar N, Koster A, Toure AML. Thermal fatigue of cast irons for automotive application. *Mater Des*. 2011;32(3):1508–1514. doi:10.1016/j.matdes.2010.10.025
29. Hayes RE, Fadic A, Mmbaga J, Najafi A. CFD modelling of the automotive catalytic converter. *Catal Today*. 2012;188(1):94–105. doi:10.1016/j.cattod.2012.03.015
30. Agrawal G, Kaisare NS, Pushpavanam S, Ramanathan K. Modeling the effect of flow mal-distribution on catalytic converter performance. *Chem Eng Sci*. 2012;71:310–320. doi:10.1016/j.ces.2011.12.041
31. Hossain MA, Badugu D, Seelu B. Multi-material and functionally graded additive manufacturing for next-generation components. *Br J Multidiscip Stud*. 2023;1(2):11–26. doi:10.32996/bjmss.2023.2.2.2
32. Marshall GJ, Mahony CP, Rhodes MJ, Daniewicz SR, Tsolas N, Thompson SM. Thermal management of vehicle cabins, surfaces, and electronics: an overview. *Engineering*. 2019;5(5):954–969. doi:10.1016/j.eng.2019.02.009
33. Yuan R, Fletcher T, Ahmedov A, *et al*. Modelling and co-simulation of hybrid vehicles: a thermal management perspective. *Appl Therm Eng*. 2020;180:115883. doi:10.1016/j.applthermaleng.2020.115883
34. Depcik C, Assanis DN. Universal heat transfer correlation for intake and exhaust flows. SAE Technical Paper 2002-01-0372; 2002. doi:10.4271/2002-01-0372
35. Li P, Chui GK, Glidewell JM, Chue TH, Lai MC. Flow network approach to vehicle underhood heat transfer. SAE Technical Paper 931073; 1993. doi:10.4271/931073
36. Clarkson R, Benjamin SF, Jasper T, Girgls NS. Integrated computational model for optimisation of monolith catalytic converters. SAE Technical Paper 931071; 1993. doi:10.4271/931071
37. Baxendale AJ. Role of CFD in exhaust system design and development. SAE Technical Paper 931072; 1993. doi:10.4271/931072
38. Wendland D. Automobile exhaust-system steady-state heat transfer. SAE Technical Paper 931085; 1993. doi:10.4271/931085
39. Chinchwade N, Barman SC, Hossain MA, Karmakar M. Coupled dynamics of ecological footprints under energy transition. *Int J Econ Finance Sustain Dev*. 2024;6(3):592–602. doi:10.31149/ijefsd.v8i1.5613
40. Morse T, Cundy M, Kytomaa H. Vehicle fires from hot surface ignition of grass and leaves. SAE Technical Paper 2017-01-1354; 2017. doi:10.4271/2017-01-1354
41. Hossain MA, Dangol S, Matheswaran K, Venkat NSG. Mechanical characterization of functionally graded metallic components. *Int J Future Eng Innov*. 2024;1(3):59–68. doi:10.54660/IJFEI.2024.1.3.59-68
42. Bai L, Cheng F, Dong Y. Ignition characteristics of automotive lubricating oil on hot surfaces. *Processes*. 2024;12(11):2522. doi:10.3390/pr12112522
43. LaPointe NR, Adams CT, Washington J. Hot surface ignition of gasoline on engine materials. SAE Technical Paper 2006-01-1013; 2006. doi:10.4271/2006-01-1013